International Forum on Aeroelasticity and Structural Dynamics
IFASD 2019
9-13 June 2019, Savannah, Georgia, USA

EFFICIENT METHOD OF AERODYNAMIC FORCE CALCULATION

Masato Tamayama[1], Shusuke Yoshida[2], and Tomohiro Yokozeki[2]

[1] Japan Aerospace Exploration Agency
Mitaka, Tokyo 1810015 JAPAN
masato@chofu.jaxa.jp

[2] The University of Tokyo
Bunkyo-ku, Tokyo 1138656 JAPAN
yoshida-shusuke834@g.ecc.u-tokyo.ac.jp
yokozeki@aastr.t.u-tokyo.ac.jp

Keywords: aerodynamic forces, unsteady, modal coordinates.

Abstract: An efficient method to calculate generalized aerodynamic forces is studied. Two kinds of structures are considered in this method: one is the original structure (Str-A), and another structure (Str-B) is the one partly having different structural characteristics from the Str-A. The concept of this method is to construct the generalized aerodynamic forces for the Str-B with the Str-A's modal information and generalized aerodynamic forces. With this method, unsteady aerodynamic calculation is conducted only for the Str-A. This method was applied to two models: a rectangular plate wing and the AGARD 445.6 wing. For both models, the expression of Str-B mode vectors improves as the FEM mesh size. The accuracy of Str-B's generalized aerodynamic forces seems far from satisfactory to introducing them to flutter analyses, and further treatment for reconstructing the Str-B mode vectors by considering artificial modal vectors should be conducted in our future study.

1 INTRODUCTION

In aeroelasticity simulations, it is possible to predict flutter condition by use of CFD applications. On the other hand, it is still expensive in view of time consumed, and it might be hard to apply CFD to every structural case to be studied in airplane design. Even if Reduced Order Modeling method is used, Full Order CFD calculations are required to construct the aerodynamic model for each structure to be varied in the design study [1], because the structural modal characteristics varies each other, and the generalized aerodynamic forces are changed among them. For the purpose improving this situation, Kim proposed the surrogate model to be available for the structures with parameter variations [2]. On the other hand, the different approach from Kim's method is proposed in this study: generalized aerodynamic forces are derived from the Full Order CFD result for a base model, and it is not needed to conduct any Full Order CFD for the structures having different parameters from the base model.

Two kinds of structures are considered in this proposed method: one is the original structure (Str-A), and another structure (Str-B) is the one partly having different structural characteristics from the Str-A. The Str-B imitates a morphing structure at the wing trailing edge. The concept of this method is to construct the generalized aerodynamic forces for the Str-B with the Str-A's modal information and generalized aerodynamic forces. When this method is applied to the flutter simulation, anyway unsteady aerodynamic calculation is required for the Str-A and

modal analysis is necessary for the Str-B, but the analysis cost is much less than doing CFD calculations for both of Str-A and Str-B.

To see the ability of the proposed method directing to a wing structure, two models are studied in this research: a rectangular plate wing and the tapered swept wing. In this paper, the derivation of this method is described at first, and then the results applied to these two wing planform models are shown. For the purpose seeing the ability of this method, low fidelity aerodynamic analysis is more favorable than introducing time-consuming CFD calculations: therefore, in this study, Doublet Lattice Method (DLM) [3, 4] is used. The results show that, for both models, the expression of Str-B mode vectors improves as the FEM mesh size. Unfortunately, the accuracy of Str-B's generalized aerodynamic forces seems far from satisfactory to introducing them to flutter analyses. In the conclusions, it is noticed that further treatment for reconstructing the Str-B mode vectors by considering artificial modal vectors should be conducted in our future study.

2 DESCRIPTION OF METHOD

Before proceeding to the description of this method, determine the model used in this section, which is used as a general model and shown in Fig.1. This model is usually introduced to

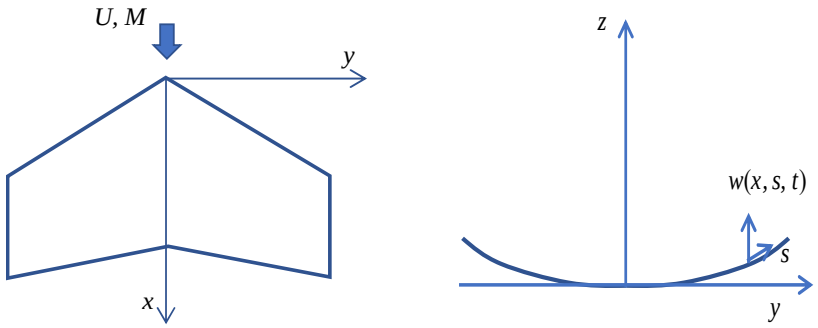

Figure 1: Coordinate system.

explain the Lifting Surface Method. According to the modal coordinate system, the aerodynamic equations are described as follows:

$$M_l\ddot{\xi}_l + M_l\omega_l^2\xi_l = \Xi_l \qquad (l = 1, 2, \cdots, m) \tag{1}$$

l is the modal index, ξ_l the modal coordinates, M_l the modal masses, ω_l the natural angular frequencies and Ξ_l the generalized aerodynamic forces. The wing displacement $w(x,s,t)$, Ξ_l, and M_l are expressed with the modal vectors, ϕ_l, as follows:

$$w(x,s,t) = \sum_{l=1}^{m} \phi_l(x,s)\xi_l(t) \tag{2}$$

$$\Xi_l = \iint_{wing\ area} P(x,s,t)\phi_l(x,s)\,dxds \tag{3}$$

$$M_l = \iint_{wing\ area} \phi_l(x,s)\rho_s(x,s)\phi_l(x,s)\,dxds \tag{4}$$

ρ_s is the airplane mass per unit area and P is the lifting pressure on the wing surface. Next, discretize the objective plane into n boxes as shown in Fig.2. Each discretized box is identified

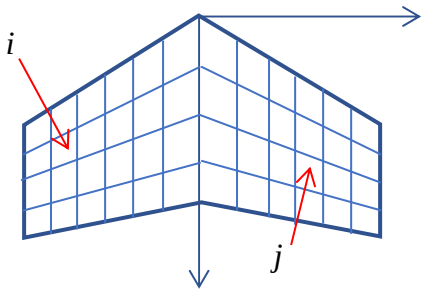

Figure 2: Discretization of wing.

sequentially with indices i or j. For each box, the representative normal velocity and lifting pressure are expressed with W_j and P_i, respectively. For a harmonic oscillation,

$$W_j(t) = \bar{W}_j e^{\hat{i}\,\omega t} \tag{5}$$

$$P_i(t) = \bar{P}_i e^{\hat{i}\,\omega t} \tag{6}$$

$\hat{i}$ expresses the imaginary unit. Determine the normalized normal velocity $\hat{W}_j$ and normalized lifting pressure $\hat{P}_i$ as follows:

$$\hat{W}_j = \frac{\bar{W}_j}{U} \tag{7}$$

$$\hat{P}_i = \frac{\bar{P}_i}{1/2\,\rho U^2} \tag{8}$$

U and ρ are the freestream velocity and density, respectively. In Ref. [3], there is a relationship between $\hat{W}_j$ and $\hat{P}_i$ as follows:

$$\hat{P}_i = \sum_{j=1}^{n} A_{ij} \hat{W}_j \tag{9}$$

A_{ij} is a function of geometrical variables, frequencies and Mach numbers. For the discretized structure, the modal coordinate system is written as follows:

$$w_j(t) = \sum_{l=1}^{n} \phi_{lj} \xi_l(t) = \sum_{l=1}^{n} \phi_{lj} \bar{\xi}_l e^{\hat{i}\,\omega t} \tag{10}$$

Here, a harmonic motion is considered for the modal coordinate, ξ_l. Between w_j and W_j, the following relation exists:

$$W_j(t) = \frac{dw_j(t)}{dt} = \sum_{l=1}^{m} \phi_{lj} \bar{\xi}_l e^{\hat{i}\,\omega t} \hat{i}\,\omega \tag{11}$$

From Eq. (5), (7) and (11), $\hat{W}_j$ is written as follows:

$$\widehat{W}_j = \sum_{l=1}^{m} \phi_{l\,j} \overline{\xi}_l \frac{\widehat{i}\,\omega}{U} \tag{12}$$

Substitute Eq. (12) to Eq. (9) and acquire next equation,

$$\widehat{P}_i = \sum_{j=1}^{n} A_{ij} \widehat{W}_j = \sum_{j=1}^{n} A_{ij} \left\{ \sum_{l=1}^{m} \phi_{l\,j} \overline{\xi}_l \frac{\widehat{i}\,\omega}{U} \right\} = \sum_{l=1}^{m} \left\{ \sum_{j=1}^{n} A_{ij} \phi_{l\,j} \right\} \overline{\xi}_l \frac{\widehat{i}\,\omega}{U} = \sum_{l=1}^{m} B_{il} \overline{\xi}_l \frac{\widehat{i}\,\omega}{U} \tag{13}$$

$$B_{il} = \sum_{j=1}^{n} A_{ij} \phi_{l\,j} \tag{14}$$

Above description is for the original structure Str-A. Now consider new structure, Str-B, which has different structural characteristics from those of Str-A. The following transformation is applied to the Str-B:

$$\begin{cases} \text{normal angular frequency} & \omega_l \Rightarrow \underline{\omega}_l \\ \text{modal vector} & \phi_l \Rightarrow \underline{\phi}_l \\ \text{modal mass} & M_l \Rightarrow \underline{M}_l \end{cases} \tag{15}$$

Then, the aeroelasticity equations, Eq. (1), for the Str-B are replaced with the followings:

$$\underline{M}_{\underline{l}} \ddot{\underline{\xi}}_{\underline{l}} + \underline{M}_{\underline{l}} \underline{\omega}_{\underline{l}}^2 \underline{\xi}_{\underline{l}} = \underline{\Xi}_{\underline{l}} \qquad \left(\underline{l} = 1, 2, \cdots, m \right) \tag{16}$$

Now, assume that the modal vectors of Str-B can be expressed with those of Str-A as follows:

$$\underline{\phi}_{\lambda i} = \sum_{l=1}^{m} \phi_{li} \cdot \delta_{\lambda l} \tag{17}$$

Here, it is assumed that the planform of Str-B doesn't change from that of Str-A. λ is the index to express mode number for Str-B. If $\left[\phi_{li}\right]$ and $\left[\underline{\phi}_{\lambda i}\right]$ are given, $\left[\delta_{\lambda l}\right]$ can be acquired from Eq. (17). With the modal vectors of Str-B, Eq. (10) can be written for the Str-B as follows:

$$\underline{w}_i(t) = \sum_{\lambda=1}^{m} \underline{\phi}_{\lambda i} \underline{\xi}_{\lambda}(t) \tag{18}$$

and, substitute Eq. (17) to Eq. (18), then,

$$\begin{aligned} \underline{w}_i(t) &= \sum_{\lambda=1}^{m} \underline{\phi}_{\lambda i} \underline{\xi}_{\lambda}(t) = \sum_{\lambda=1}^{m} \left\{ \sum_{l=1}^{m} \phi_{li} \delta_{\lambda l} \right\} \underline{\xi}_{\lambda} \\ &= \sum_{\lambda=1}^{m} \left\{ \phi_{1i} \delta_{\lambda 1} \underline{\xi}_{\lambda} + \phi_{2i} \delta_{\lambda 2} \underline{\xi}_{\lambda} + \cdots + \phi_{mi} \delta_{\lambda m} \underline{\xi}_{\lambda} \right\} \\ &= \phi_{1i} \delta_{11} \underline{\xi}_1 + \phi_{2i} \delta_{12} \underline{\xi}_1 + \cdots + \phi_{mi} \delta_{1m} \underline{\xi}_1 \\ &\quad + \phi_{1i} \delta_{21} \underline{\xi}_2 + \phi_{2i} \delta_{22} \underline{\xi}_2 + \cdots + \phi_{mi} \delta_{2m} \underline{\xi}_2 \\ &\quad + \cdots \\ &\quad + \phi_{1i} \delta_{m1} \underline{\xi}_m + \phi_{2i} \delta_{m2} \underline{\xi}_m + \cdots + \phi_m \delta_{mm} \underline{\xi}_m \end{aligned} \tag{19}$$

After gathering $\underline{\xi}_1, \underline{\xi}_2, \cdots, \underline{\xi}_m$ into the vector $\left\{\underline{\xi}\right\}^T = \left\{\underline{\xi}_1, \underline{\xi}_2, \cdots, \underline{\xi}_m\right\}$, the terms in Eq. (19) is rearranged as follows:

$$\begin{cases} \phi_{1i}\left(\delta_{11}\underline{\xi}_1 + \delta_{21}\underline{\xi}_2 + \cdots + \delta_{m1}\underline{\xi}_m\right) &= \phi_{1i}\left\{\delta_{11}, \delta_{21}, \cdots, \delta_{m1}\right\}\left\{\underline{\xi}\right\} \\ \phi_{2i}\left(\delta_{12}\underline{\xi}_1 + \delta_{22}\underline{\xi}_2 + \cdots + \delta_{m2}\underline{\xi}_m\right) &= \phi_{2i}\left\{\delta_{12}, \delta_{22}, \cdots, \delta_{m2}\right\}\left\{\underline{\xi}\right\} \\ \vdots & \\ \phi_{mi}\left(\delta_{1m}\underline{\xi}_1 + \delta_{2m}\underline{\xi}_2 + \cdots + \delta_{mm}\underline{\xi}_m\right) &= \phi_{mi}\left\{\delta_{1m}, \delta_{2m}, \cdots, \delta_{mm}\right\}\left\{\underline{\xi}\right\} \end{cases} \tag{20}$$

Integrating these equations for i=1~n into one equation, and Eq. (19) is replaced as follows:

$$\left\{\underline{w}\right\} = \begin{Bmatrix} \underline{w}_1 \\ \underline{w}_2 \\ \vdots \\ \underline{w}_n \end{Bmatrix} = \begin{bmatrix} \phi_{11} & \phi_{21} & \cdots & \phi_{m1} \\ \phi_{12} & \phi_{22} & \cdots & \phi_{m2} \\ \vdots & \vdots & \ddots & \vdots \\ \phi_{1n} & \phi_{2n} & \cdots & \phi_{mn} \end{bmatrix} \begin{bmatrix} \delta_{11} & \delta_{21} & \cdots & \delta_{m1} \\ \delta_{12} & \delta_{22} & \cdots & \delta_{m2} \\ \vdots & \vdots & \ddots & \vdots \\ \delta_{1m} & \delta_{2m} & \cdots & \delta_{mm} \end{bmatrix} \left\{\underline{\xi}\right\} \tag{21}$$

After introducing the following expressions,

$$\left[\phi\right] = \left[\left\{\phi_1\right\}\left\{\phi_2\right\}\cdots\left\{\phi_m\right\}\right] = \begin{bmatrix} \phi_{11} & \phi_{21} & \cdots & \phi_{m1} \\ \phi_{12} & \phi_{22} & \cdots & \phi_{m2} \\ \vdots & \vdots & \ddots & \vdots \\ \phi_{1n} & \phi_{2n} & \cdots & \phi_{mn} \end{bmatrix} \tag{22}$$

$$\left\{\underline{\underline{\xi}}\right\} = \left[\delta\right]\left\{\underline{\xi}\right\}, \quad \left[\delta\right] = \begin{bmatrix} \delta_{11} & \delta_{21} & \cdots & \delta_{m1} \\ \delta_{12} & \delta_{22} & \cdots & \delta_{m2} \\ \vdots & \vdots & \ddots & \vdots \\ \delta_{1m} & \delta_{2m} & \cdots & \delta_{mm} \end{bmatrix} \tag{23}$$

Eq. (21) is replaced with the following equation:

$$\left\{\underline{w}\right\} = \left[\phi\right]\left\{\underline{\underline{\xi}}\right\} \tag{24}$$

If a harmonic oscillation is considered, $\left\{\underline{w}\right\} = \left\{\overline{w}\right\}e^{\hat{i}\omega t}$ and $\left\{\underline{\underline{\xi}}\right\} = \left\{\overline{\underline{\xi}}\right\}e^{\hat{i}\omega t}$, the following amplitude equation is acquired,

$$\left\{\overline{w}\right\} = \left[\phi\right]\left\{\overline{\underline{\xi}}\right\} \tag{25}$$

A_{ij} in Eq. (9) is not a function of structural parameters, and, therefore, A_{ij} is still available for the Str-B. Then, the lifting pressure amplitude, $\underline{\hat{P}}_i$ for the Str-B is expressed with the normalized normal velocity for the Str-B, $\underline{\hat{W}}_j$, as follows:

$$\underline{\hat{P}}_i = \sum_{j=1}^{n} A_{ij}\underline{\hat{W}}_j = \sum_{j=1}^{n} A_{ij}\sum_{l=1}^{m}\left(\phi_{lj}\overline{\underline{\xi}}_l\frac{\hat{i}\omega}{U}\right) = \frac{\hat{i}\omega}{U}\sum_{l=1}^{m}\left(\sum_{j=1}^{n} A_{ij}\phi_{lj}\right)\overline{\underline{\xi}}_l = \frac{\hat{i}\omega}{U}\sum_{l=1}^{m} B_{il}\overline{\underline{\xi}}_l \tag{26}$$

Next, consider the generalized aerodynamic force amplitudes. Here, the γ^{th} mode generalized aerodynamic force is focused for the ease of proceeding derivation. And moreover, as the lifting pressure, the σ^{th} term of $\left\{\underline{\hat{P}}\right\}$ is especially decomposed from Eq. (26) and focused.

$$
\begin{aligned}
\underline{\underline{\Xi}}_{\gamma\sigma} &= \iint_{\text{wing area}} \frac{1}{2}\rho U^2 \underline{\hat{P}}^{\sigma}(x,s)\underline{\phi}_{\gamma}(x,s)\,dxds \\
&\cong \frac{1}{2}\rho U^2 \sum_{j=1}^{n} \underline{\hat{P}}_j^{\sigma} \underline{\phi}_{\gamma j} S_j \\
&= \frac{1}{2}\rho U^2 \sum_{j=1}^{n} \left(\frac{\hat{i}\omega}{U} B_{j\sigma} \underline{\underline{\xi}}_{\sigma} \right) \left(\sum_{l=1}^{m} \phi_{lj} \cdot \delta_{\gamma l} \right) S_j \\
&= \frac{1}{2}\rho U^2 \frac{\hat{i}\omega}{U} \underline{\underline{\xi}}_{\sigma} \sum_{j=1}^{n} \left(\phi_{1j}\delta_{\gamma 1} + \phi_{2j}\delta_{\gamma 2} + \cdots + \phi_{mj}\delta_{\gamma m} \right) B_{j\sigma} S_j \\
&= \frac{1}{2}\rho U \hat{i}\omega \underline{\underline{\xi}}_{\sigma} \begin{Bmatrix} \delta_{\gamma 1} & \delta_{\gamma 2} & \cdots & \delta_{\gamma m} \end{Bmatrix} \begin{bmatrix} \phi_{11} & \phi_{12} & \cdots & \phi_{1n} \\ \phi_{21} & \phi_{22} & \cdots & \phi_{2n} \\ \vdots & \vdots & \ddots & \vdots \\ \phi_{m1} & \phi_{m2} & \cdots & \phi_{mn} \end{bmatrix} \begin{bmatrix} S_1 & 0 & \cdots & 0 \\ 0 & S_2 & \ddots & \vdots \\ \vdots & \ddots & \ddots & 0 \\ 0 & \cdots & 0 & S_n \end{bmatrix} \begin{Bmatrix} B_{1\sigma} \\ B_{2\sigma} \\ \vdots \\ B_{n\sigma} \end{Bmatrix} \\
&= \underline{\underline{\xi}}_{\sigma} \left(\frac{1}{2}\rho U \hat{i}\omega \begin{Bmatrix} \delta_{\gamma 1} & \delta_{\gamma 2} & \cdots & \delta_{\gamma m} \end{Bmatrix} [\phi]^T [S] \begin{Bmatrix} B_{1\sigma} \\ B_{2\sigma} \\ \vdots \\ B_{n\sigma} \end{Bmatrix} \right) \\
&= \underline{\underline{\xi}}_{\sigma} \underline{Q}_{\gamma\sigma}
\end{aligned}
\tag{27}
$$

Here, the diagonal matrix composed of box areas is determined as [S],

$$
[S] = \begin{bmatrix} S_1 & 0 & \cdots & 0 \\ 0 & S_2 & \ddots & \vdots \\ \vdots & \ddots & \ddots & 0 \\ 0 & \cdots & 0 & S_n \end{bmatrix} \tag{28}
$$

$\underline{Q}_{\gamma\sigma}$ is the generalized aerodynamic force coefficient per unit $\underline{\underline{\xi}}_{\sigma}$. If the original structure is considered, the generalized aerodynamic force $\underline{\underline{\Xi}}_{\gamma\sigma}$ can be written as same as Eq. (27):

$$
\underline{\underline{\Xi}}_{\gamma\sigma} = \underline{\xi}_{\sigma} \left(\frac{1}{2}\rho U \hat{i}\omega \begin{Bmatrix} 0 & \cdots & 1\left(\gamma^{th}\ column\right) & \cdots & 0 \end{Bmatrix} [\phi]^T [S] \begin{Bmatrix} B_{1\sigma} \\ B_{2\sigma} \\ \vdots \\ B_{n\sigma} \end{Bmatrix} \right) = \underline{\xi}_{\sigma} Q_{\gamma\sigma} \tag{29}
$$

Then, $\underline{Q}_{\gamma\sigma}$ can be written with $Q_{\gamma\sigma}$ as follows:

$$
\begin{aligned}
\underline{Q}_{\gamma\sigma} &= \frac{1}{2}\rho U\hat{i}\omega\begin{Bmatrix}\delta_{\gamma 1} & \delta_{\gamma 2} & \cdots & \delta_{\gamma m}\end{Bmatrix}[\phi]^T[S]\begin{Bmatrix}B_{1\sigma}\\ B_{2\sigma}\\ \vdots\\ B_{n\sigma}\end{Bmatrix} \\
&= \frac{1}{2}\rho U\hat{i}\omega\delta_{\gamma 1}\begin{Bmatrix}1 & 0 & \cdots & 0\end{Bmatrix}[\phi]^T[S]\begin{Bmatrix}B_{1\sigma}\\ B_{2\sigma}\\ \vdots\\ B_{n\sigma}\end{Bmatrix} + \cdots + \frac{1}{2}\rho U\hat{i}\omega\delta_{\gamma m}\begin{Bmatrix}0 & 0 & \cdots & 1\end{Bmatrix}[\phi]^T[S]\begin{Bmatrix}B_{1\sigma}\\ B_{2\sigma}\\ \vdots\\ B_{n\sigma}\end{Bmatrix} \\
&= \delta_{\gamma 1}Q_{1\sigma} + \delta_{\gamma 2}Q_{2\sigma} + \cdots + \delta_{\gamma m}Q_{m\sigma} \\
&= \sum_{l=1}^{m}\delta_{\gamma l}Q_{l\sigma}
\end{aligned}
\tag{30}
$$

Finally, the γ^{th} mode generalized aerodynamic force can be derived by taking the summation of Eq. (27) from σ=1 through m.

$$
\underline{\underline{\Xi}}_{\gamma} = \sum_{\sigma=1}^{m}\underline{\underline{\xi}}_{\sigma}\left(\sum_{l=1}^{m}\delta_{\gamma l}Q_{l\sigma}\right) \tag{31}
$$

3 ANALYSIS MODELS

3.1 Rectangular Plate Wing (Wing-Rect)

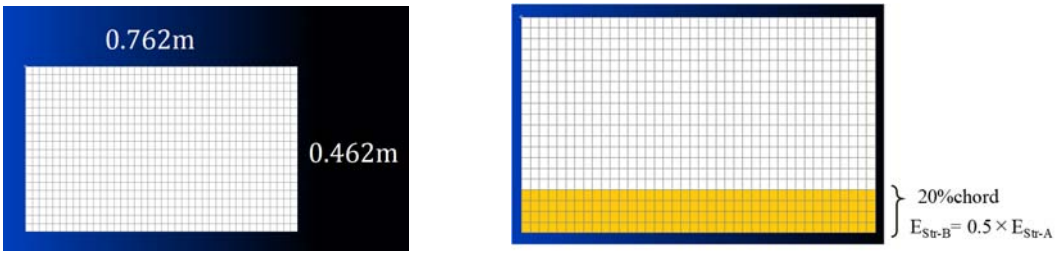

(a) Str-$A_{\text{Wing-Rect}}$ (b) Str-$B_{\text{Wing-Rect}}$

Figure 3: Structural mesh for Wing-Rect.

Figure 3(a) shows the rectangular plate wing, calling this wing as 'Wing-Rect.' The chord and semi-span lengths are 0.462m and 0.762m, respectively. The thickness of the plate is 0.0122m everywhere. The plate is applied with a constraint forbidding motions in six degrees of freedom at its root. The material is A7075. The structural model is generated with shell elements. The sizes of discretization in chordwise and spanwise directions are varied to see its influences on the accuracy of method. Three patterns of mesh sizes are studied: 10 in chordwise × 20 in spanwise, 20×40, and 40×80. In this research, the aerodynamic forces are calculated with DLM: for the aerodynamic boxes, the structural mesh is also used for DLM. The air density is set to 0.5 kg/m^3. The wing mentioned above is the original structure, Str-$A_{\text{wing-Rect}}$. As for the Str-$B_{\text{wing-Rect}}$, the 20% chord area from the trailing edge is applied with reduced Young's modulus by 50% from that of A7075 (Fig.3(b)).

3.2 Tapered Swept Wing (Wing-Swept)

To see the influence of model planform, a tapered swept wing, calling this wing as 'Wing-Swept,' is also applied with the proposed method. The planform is the same as AGARD 445.6 model [5]. The model is shown in Fig.4. The root and tip chord lengths are 0.462m and 0.366m,

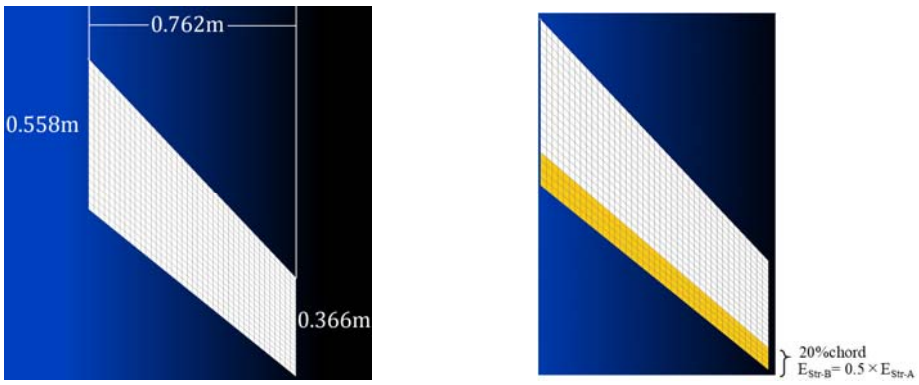

(a) Str-$A_{Wing\text{-}Swept}$ (b) Str-$B_{Wing\text{-}Swept}$

Figure 4: Structural mesh for Wing- Swept.

respectively, and the mean chord length is 0.462m. The span length is 0.762m. The swept angle is 45° measured on the 25% chord line. The same constraint as the Wing-Rect is applied to the root of Wing-Swept. The cross section is NASA65A004 airfoil. As same as the Wing-Rect, the material is A7075, and the sizes of structural model discretization are set to chordwise 10× spanwise 20, 20×40, and 40×80. These meshes are also used for DLM as aerodynamic boxes. The air density is set to 0.5 kg/m^3. As for the Str-$B_{Wing\text{-}Swept}$, the 20% chord area from the trailing edge is applied with reduced Young's modulus by 50% from that of A7075 (Fig.4(b)).

4 RESULTS AND DISCUSSIONS

4.1 Wing-Rect

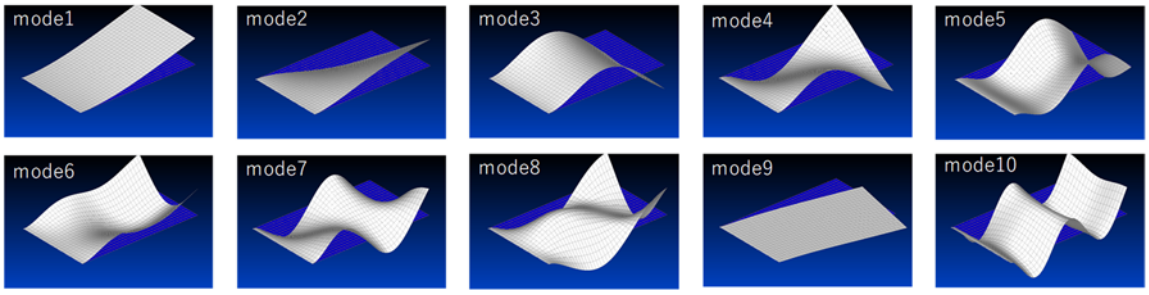

Figure 5: Mode shapes for Str-$A_{Wing\text{-}Rect}$.

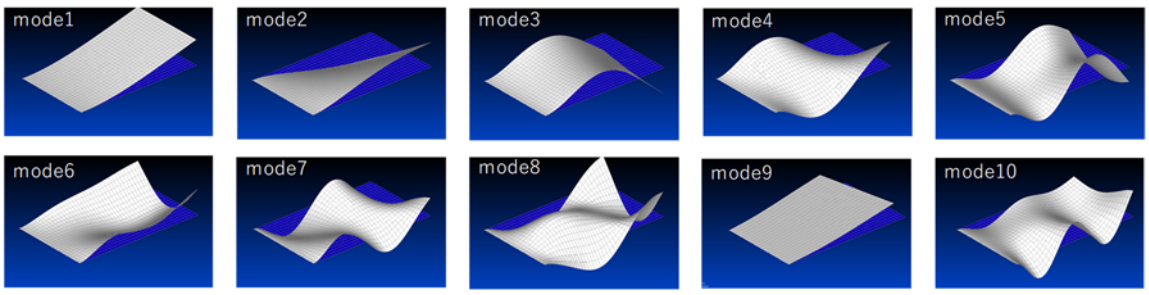

Figure 6: Mode shapes for Str-$B_{Wing\text{-}Rect}$.

The modal vectors for the Str-A$_{\text{Wing-Rect}}$ and Str-B$_{\text{Wing-Rect}}$ are shown in Fig.5 and 6, respectively. These are calculated with MSC-NASTRAN. In both figures, the mode 9 is the in-plane mode, and, therefore, the mode 9 is omitted in the following discussions.

Eq. (17) is applied to the mode vectors $[\phi]$ of Str-A$_{\text{Wing-Rect}}$ and $\left[\underline{\phi}\right]$ of Str-B$_{\text{Wing-Rect}}$. Call this calculated $\left[\underline{\phi}\right]$ as $\left[\underline{\phi}_{true}\right]$. After calculating $[\delta]$ in Eq. (17), $\left[\underline{\phi}\right]$ is reconstructed, call this modal vector matrix as $\left[\underline{\phi}_{approximated}\right]$, and compare this matrix with $\left[\underline{\phi}_{true}\right]$. Here, the error factor determined as following equation is introduced.

$$e_{\lambda} = \frac{\left\| \left\{\underline{\phi}_{\lambda}\right\}_{true} - \left\{\underline{\phi}_{\lambda}\right\}_{approximated} \right\|}{\left\| \left\{\underline{\phi}_{\lambda}\right\}_{true} \right\|} \tag{32}$$

e_{λ} is calculated for each mode as shown in Tab.1. e_{λ} decreases as the mesh size, though the higher mode shows relatively large value even if the mesh size is increased.

Table 1: Error factor e_{λ} for Wing-Rect.

Mode	*Mesh size 10×20*	*20×40*	*40×80*
1	2.93E-03	7.53E-04	2.02E-04
2	1.53E-02	3.92E-03	1.35E-03
3	1.18E-02	2.94E-03	1.09E-03
4	1.99E-02	6.72E-03	4.80E-03
5	2.72E-02	9.91E-03	7.63E-03
6	4.18E-02	1.69E-02	1.43E-02
7	3.06E-02	1.31E-02	1.14E-02
8	5.16E-02	2.82E-02	2.65E-02
10	2.19E-01	2.69E-01	4.14E-01

With matrix $[\delta]$ and the generalized aerodynamic forces coefficient matrix $[Q]$ for the Str-A$_{\text{Wing-Rect}}$, the matrix $\left[\underline{Q}\right]$ for the Str-B$_{\text{Wing-Rect}}$ is acquired from Eq. (30). The error factors determined as following equations are introduced to see the accuracy of $\left[\underline{Q}\right]$.

$$\begin{cases} e_{\gamma\sigma\_\text{Real}} = \dfrac{\left|\text{Re}\left(\underline{Q}_{\gamma\sigma\sim true}\right) - \text{Re}\left(\underline{Q}_{\gamma\sigma\sim approximated}\right)\right|}{\sqrt{\left|\text{Re}\left(\underline{Q}_{\gamma\sigma\sim true}\right) \times \text{Re}\left(\underline{Q}_{\gamma\sigma\sim approximated}\right)\right|}} \\ e_{\gamma\sigma\_\text{Imag}} = \dfrac{\left|\text{Im}\left(\underline{Q}_{\gamma\sigma\sim true}\right) - \text{Im}\left(\underline{Q}_{\gamma\sigma\sim approximated}\right)\right|}{\sqrt{\left|\text{Im}\left(\underline{Q}_{\gamma\sigma\sim true}\right) \times \text{Im}\left(\underline{Q}_{\gamma\sigma\sim approximated}\right)\right|}} \end{cases} \tag{33}$$

The elements of $\left[\underline{Q}\right]$ are complex, and, therefore, each of real and imaginary parts is calculated individually. The result is shown in Tab.2(a) through Tab.2(f). The level of error magnitude is distinguished by the cells' background colors in the tables.

Table 2 (a): Error factor $e_{\gamma\sigma\_Real}$ for Wing-Rect, mesh size 10×20

blue…～0.05 light blue…0.05～0.1 green…0.1～0.3 yellow…0.3～0.5 red…0.5～

Real	σ=1	2	3	4	5	6	7	8	10
γ=1	4.33E-02	3.19E-02	7.94E-02	2.62E-02	9.36E-02	9.86E-02	1.23E-01	5.61E-02	4.68E-01
2	4.32E-02	3.05E-02	5.66E-02	1.20E-01	6.47E-02	7.86E-02	1.22E-01	3.71E-01	6.72E-01
3	5.74E-02	1.04E-01	2.51E-02	2.84E-02	3.63E-01	3.88E-02	1.49E-01	1.79E-01	1.99E-01
4	5.84E-02	1.11E-01	8.62E-02	2.08E-02	1.51E-01	4.39E-02	3.73E-01	2.00E-03	1.22E-01
5	3.42E-01	5.37E-01	3.65E-01	4.02E-01	1.06E+00	3.38E-01	1.35E-01	3.15E-01	2.40E+00
6	1.10E-01	1.41E-01	1.66E-01	1.58E-01	8.27E-02	1.18E-01	3.64E-01	2.35E-01	1.47E-01
7	4.68E-01	2.67E+00	9.40E-01	5.22E-01	2.06E+00	1.07E-01	1.69E-01	2.43E-01	2.11E-01
8	1.39E-01	1.84E-01	1.75E-01	9.31E-02	2.48E-02	2.01E-01	5.02E-02	4.89E-02	8.08E-02
10	2.28E-01	4.65E+00	3.73E-01	2.37E-01	6.24E-01	2.12E-01	5.24E-02	6.15E-01	4.28E-01

Table 2 (b): Error factor $e_{\gamma\sigma\_Real}$ for Wing-Rect, mesh size 20×40

Real	σ=1	2	3	4	5	6	7	8	10
γ=1	2.02E-02	1.06E-03	3.42E-02	2.99E-03	5.36E-02	6.47E-02	7.05E-02	3.81E-02	3.44E-01
2	1.61E-02	2.66E-02	2.73E-02	1.24E-01	2.76E-02	4.85E-02	7.95E-02	3.28E-01	1.04E+00
3	6.31E-02	7.11E-02	5.59E-02	9.91E-03	3.08E-01	5.47E-02	1.23E-01	1.34E-01	1.53E-01
4	6.75E-02	1.00E-01	1.47E-01	9.57E-03	1.29E-01	8.91E-02	3.57E-01	3.59E-02	1.54E-01
5	3.72E-01	6.00E-01	4.04E-01	3.65E-01	1.28E+00	3.83E-01	6.71E-02	3.10E-01	2.09E+00
6	8.79E-02	9.55E-02	1.28E-01	1.94E-01	4.46E-02	8.29E-02	4.01E-01	1.95E-01	8.10E-02
7	4.28E-01	6.05E+00	8.31E-01	5.04E-01	2.04E+00	4.10E-01	1.82E-01	2.85E-01	2.53E-01
8	1.02E-01	1.48E-01	1.36E-01	3.51E-02	7.82E-02	1.61E-01	1.09E-01	1.21E-02	3.58E-02
10	2.29E-01	2.95E+00	3.74E-01	2.35E-01	5.96E-01	1.77E-01	5.55E-04	5.80E-01	3.73E-01

Table 2 (c): Error factor $e_{\gamma\sigma\_Real}$ for Wing-Rect, mesh size 40×80

Real	σ=1	2	3	4	5	6	7	8	10
γ=1	1.36E-02	9.12E-03	2.25E-02	9.87E-03	4.37E-02	5.65E-02	5.78E-02	3.50E-02	3.15E-01
2	9.79E-03	2.58E-02	2.06E-02	1.23E-01	1.89E-02	4.22E-02	7.09E-02	3.16E-01	1.30E+00
3	6.29E-02	6.19E-02	6.11E-02	1.93E-02	2.81E-01	5.39E-02	1.33E-01	1.22E-01	1.37E-01
4	7.14E-02	9.71E-02	1.68E-01	6.31E-03	1.30E-01	1.05E-01	3.47E-01	4.62E-02	1.69E-01
5	3.80E-01	6.14E-01	4.15E-01	3.53E-01	1.42E+00	3.96E-01	5.16E-02	3.02E-01	1.92E+00
6	8.34E-02	8.80E-02	1.20E-01	2.04E-01	3.45E-02	7.48E-02	4.08E-01	1.84E-01	6.28E-02
7	4.29E-01	2.79E+00	7.93E-01	4.95E-01	2.05E+00	5.69E-01	1.89E-01	2.94E-01	2.65E-01
8	9.27E-02	1.38E-01	1.24E-01	2.26E-02	9.50E-02	1.49E-01	1.20E-01	2.90E-03	2.29E-02
10	2.17E-01	2.66E+00	3.69E-01	2.54E-01	5.82E-01	1.67E-01	1.95E-02	5.71E-01	3.45E-01

Table 2 (d): Error factor $e_{\gamma\sigma\_\text{Imaginary}}$ for Wing-Rect, mesh size 10×20

Imaginary	σ=1	2	3	4	5	6	7	8	10
γ=1	1.23E-02	1.86E-02	2.23E-02	4.28E-02	8.15E-01	2.80E-02	7.53E-02	8.67E-02	6.69E-02
2	1.68E-02	2.38E-02	2.79E-01	3.10E-01	4.78E-02	5.23E-02	4.59E-02	1.02E-01	5.11E-01
3	9.41E-02	6.15E-02	2.52E-02	3.97E-02	3.37E-01	4.01E-01	3.32E-01	3.68E-01	2.30E-01
4	1.67E-01	2.17E-01	2.05E-02	1.14E-01	2.87E-01	6.66E-02	8.60E-01	6.58E-02	8.25E-02
5	4.57E-01	5.08E-01	1.06E+00	1.89E-01	8.51E-02	5.53E-02	1.86E-01	2.93E-02	4.46E-01
6	1.02E-01	6.20E-02	8.74E-02	4.92E-01	4.48E-01	3.54E-01	1.57E-01	9.27E-02	8.50E-01
7	1.46E+00	1.11E+00	1.12E+00	1.09E+00	1.01E+00	3.27E+00	5.75E-01	8.37E-03	1.46E-01
8	2.78E+00	1.45E-01	8.69E-03	4.02E-02	8.07E-02	3.29E-01	5.94E-02	4.31E-01	1.99E+00
10	1.84E+00	1.55E-01	2.92E-01	3.68E-01	1.68E-01	1.32E+01	7.78E-01	7.39E-02	1.48E-01

Table 2 (e): Error factor $e_{\gamma\sigma\_\text{Imaginary}}$ for Wing-Rect, mesh size 20×40

Imaginary	σ=1	2	3	4	5	6	7	8	10
γ=1	1.31E-02	9.07E-03	1.28E-02	8.50E-03	1.68E-01	1.25E-01	3.03E-02	5.19E-02	9.75E-02
2	1.86E-02	1.12E-02	2.27E-01	2.63E-01	1.53E-02	2.12E-02	9.96E-03	7.08E-02	7.27E-01
3	9.00E-02	6.44E-02	2.74E-02	2.45E-02	3.26E-01	4.25E-01	3.12E-01	7.16E+00	7.65E-01
4	1.57E-01	2.40E-01	2.66E-02	1.23E-01	2.63E-01	2.51E-02	7.54E-01	3.15E-02	4.22E-02
5	4.65E-01	5.32E-01	1.05E+00	1.91E-01	7.07E-02	1.34E-01	1.59E-01	2.40E+00	3.52E-01
6	1.03E-01	5.97E-02	8.50E-02	4.73E-01	4.69E-01	3.45E-01	1.77E-01	9.21E-02	6.66E-01
7	1.11E+00	7.91E-01	1.07E+00	1.02E+00	1.24E+00	6.71E-01	5.72E-01	5.45E-02	9.95E-02
8	8.87E-01	1.30E-01	2.98E-03	4.02E-02	8.49E-02	3.21E-01	6.48E-02	4.37E-01	2.35E+00
10	2.22E+00	1.62E-01	4.16E-01	3.73E-01	1.84E-01	1.97E+00	6.62E-01	2.09E-02	1.29E-01

Table 2 (f): Error factor $e_{\gamma\sigma\_\text{Imaginary}}$ for Wing-Rect, mesh size 40×80

Imaginary	σ=1	2	3	4	5	6	7	8	10
γ=1	1.33E-02	6.68E-03	1.11E-02	2.99E-03	1.14E-01	2.08E-01	2.03E-02	4.38E-02	9.31E-02
2	1.92E-02	8.14E-03	2.12E-01	2.46E-01	7.33E-03	1.40E-02	7.10E-04	6.35E-02	8.83E-01
3	8.71E-02	6.36E-02	2.77E-02	2.08E-02	3.20E-01	4.51E-01	3.01E-01	1.54E+00	6.99E-01
4	1.51E-01	2.47E-01	2.90E-02	1.24E-01	2.54E-01	1.37E-02	7.13E-01	2.30E-02	3.19E-02
5	4.68E-01	5.49E-01	1.03E+00	1.90E-01	7.12E-02	2.87E-01	1.54E-01	3.01E+00	3.32E-01
6	1.05E-01	5.87E-02	8.63E-02	4.66E-01	4.59E-01	3.79E-01	1.78E-01	8.66E-02	6.07E-01
7	9.53E-01	6.37E-01	1.04E+00	9.88E-01	1.47E+00	4.41E-01	5.71E-01	6.96E-02	8.40E-02
8	6.86E-01	1.26E-01	1.28E-03	3.98E-02	8.41E-02	3.20E-01	6.46E-02	4.52E-01	2.20E+00
10	2.52E+00	1.62E-01	5.06E-01	3.68E-01	2.02E-01	1.55E+00	6.33E-01	3.04E-02	1.25E-01

Even if the mesh size is increased, the proposed method doesn't show good accuracy for the Wing-Rect, though the generalized aerodynamic forces of lower modes show better accuracy. The considerable reason for this is the insufficient number of modes to be considered in this study. Adding to this reason, the result might be also influenced by the unusual planform of Wing-Rect. Therefore, the Wing-Swept is studied next.

4.2 Wing-Swept

The modal vectors for the Str-A$_{\text{Wing-Swept}}$ and Str-B$_{\text{Wing-Swept}}$ are shown in Fig.7 and 8, respectively. In both figures, the mode 6 is the in-plane mode, and, therefore, the mode 6 is omitted in the following discussions.

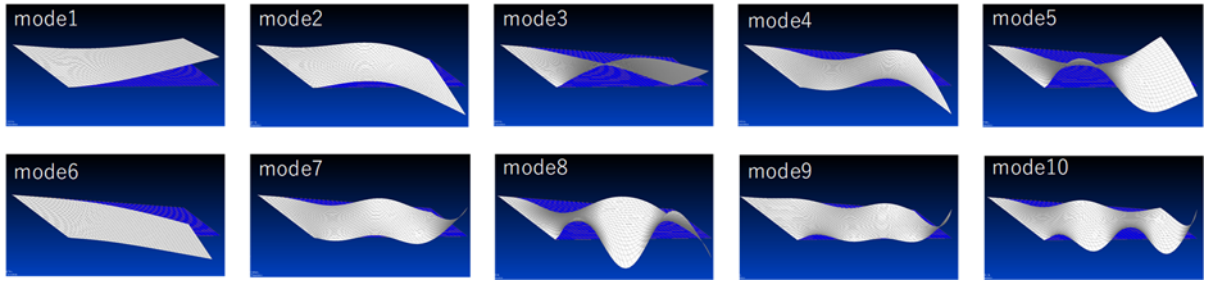

Figure 7: Mode shapes for Str-A$_{\text{Wing-Swept}}$.

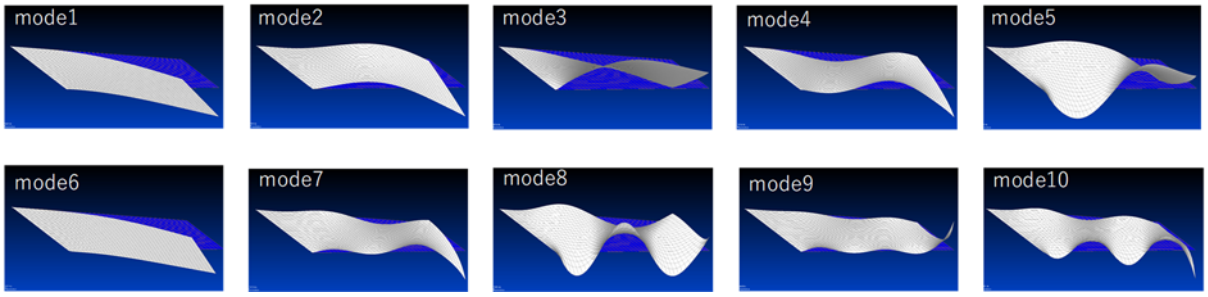

Figure 8: Mode shapes for Str-B$_{\text{Wing-Swept}}$.

Table 3: Error factor e_λ for Wing-Swept.

Mode	*Mesh size 10×20*	*20×40*	*40×80*
1	4.09E-03	1.12E-03	3.16E-04
2	1.65E-02	4.60E-03	1.49E-03
3	2.18E-02	7.13E-03	3.55E-03
4	3.45E-02	1.15E-02	6.19E-03
5	4.05E-02	1.80E-02	3.46E-02
7	7.50E-02	2.95E-02	2.01E-02
8	8.45E-02	5.84E-02	4.45E-02
9	1.51E-01	8.30E-02	6.78E-02
10	1.64E-01	1.14E-01	9.34E-02

As same as the Wing-Rect, e_λ is calculated for each mode as shown in Tab.3. e_λ decreases as the mesh size.

The error factors determined with Eq. (33) are calculated to see the accuracy of the proposed method as shown in Tab.4(a) through Tab.4(f). As the mesh size is increased, the proposed method shows better accuracy. The applicability of this method to the Wing-Swept is higher than to the Wing-Rect. The shape of mode vectors might affect the accuracy difference between these two wings: the chordwise camber deformation seems much stronger in the Wing-Rect

modes than those of Wing-Swept. Even for the Wing-Swept, the accuracy level is not enough. This might be arisen from insufficient accuracy of expressing $\left[\underline{\phi}\right]$ with $\left[\phi\right]$. For the next study, we are planning to introduce artificial mode vectors into this proposed method.

Table 4 (a): Error factor $e_{\gamma\sigma\_\mathrm{Real}}$ for Wing-Swept, mesh size 10×20
blue…～0.05 light blue…0.05～0.1 green…0.1～0.3 yellow…0.3～0.5 red…0.5～

Real	σ=1	2	3	4	5	7	8	9	10
γ=1	3.73E-02	4.00E-02	6.84E-02	7.32E-02	1.28E-01	1.07E-01	1.90E-01	1.92E-01	4.33E-01
2	1.03E-02	1.68E-02	2.38E-02	8.41E-02	2.11E-01	1.35E-01	2.00E-01	2.11E-01	6.90E-01
3	7.73E-03	6.74E-03	7.00E-02	1.10E-01	9.81E-02	1.34E-01	1.82E-01	2.47E-01	4.56E-01
4	8.71E-03	9.48E-03	9.24E-02	1.34E-01	6.48E-02	1.83E-01	8.06E-02	2.53E-01	3.06E-01
5	9.16E-03	8.16E-02	2.49E+00	2.61E-01	1.51E+00	1.37E-01	8.07E-02	2.58E-01	3.28E-01
7	5.61E-02	6.51E-02	2.56E-01	2.40E-01	1.70E-01	2.99E+00	2.21E-01	3.39E-01	3.37E-01
8	1.59E-01	4.18E-02	1.66E-01	1.49E+00	1.29E-01	8.99E-01	7.54E-01	3.09E-01	1.94E-01
9	8.15E-02	1.03E-01	1.11E-01	2.04E-01	1.18E-01	7.01E-01	2.52E-01	4.74E-01	5.15E-01
10	1.04E-01	1.59E-01	3.63E-01	1.32E-01	1.02E+00	3.41E-01	4.59E-02	8.39E-01	7.20E-01

Table 4 (b): Error factor $e_{\gamma\sigma\_\mathrm{Real}}$ for Wing-Swept, mesh size 20×40

Real	σ=1	2	3	4	5	7	8	9	10
γ=1	1.06E-02	1.05E-02	3.33E-02	2.71E-02	6.89E-02	5.23E-02	7.92E-03	1.05E-01	5.72E-01
2	4.22E-03	2.28E-02	5.27E-03	5.20E-02	1.98E-01	8.99E-02	2.13E-01	1.73E-01	4.93E-01
3	9.44E-03	1.33E-02	4.37E-02	2.47E-02	3.32E-02	3.01E-02	9.16E-01	8.71E-02	7.97E-01
4	1.45E-02	1.91E-02	2.68E-02	1.05E-01	3.76E-02	1.43E-01	2.93E-01	2.26E-01	2.85E-01
5	3.32E-02	7.57E-03	3.00E-01	3.16E-02	3.61E+00	7.74E-02	1.68E-02	1.03E-01	3.89E-01
7	7.84E-02	4.81E-02	2.43E+00	1.58E-01	1.12E-01	7.94E-01	1.49E-01	3.15E-01	2.43E-01
8	1.65E-01	6.53E-02	1.24E-01	1.15E+00	9.44E-02	4.05E-01	1.58E+00	4.54E-01	1.64E-01
9	6.12E-02	7.15E-02	6.35E-02	1.96E-01	1.03E-02	4.55E-01	4.14E-01	7.19E-01	5.79E-01
10	1.08E-01	2.95E-01	2.57E-01	2.12E-01	1.49E+00	3.08E-01	4.54E-02	8.59E-01	1.04E+00

Table 4 (c): Error factor $e_{\gamma\sigma\_\mathrm{Real}}$ for Wing-Swept, mesh size 40×80

Real	σ=1	2	3	4	5	7	8	9	10
γ=1	4.81E-03	4.95E-03	2.25E-02	1.89E-02	4.66E-02	4.09E-02	4.12E-02	1.03E-01	3.81E-01
2	7.84E-03	2.43E-02	3.44E-04	4.25E-02	1.98E-01	7.66E-02	1.90E-01	1.62E-01	3.77E-01
3	9.30E-03	1.64E-02	3.27E-02	1.42E-02	1.07E-02	1.66E-02	2.21E+00	8.74E-02	7.02E-01
4	1.15E-02	2.37E-02	8.24E-03	9.08E-02	3.01E-02	1.28E-01	1.97E-01	2.08E-01	2.22E-01
5	3.62E-02	6.10E-03	1.59E-01	2.80E-01	1.37E+00	6.37E-02	2.61E-02	1.18E-01	5.85E-01
7	1.06E-01	3.03E-02	6.54E-01	1.16E-01	8.96E-02	1.43E+00	1.32E-01	3.09E-01	2.07E-01
8	1.76E-01	8.39E-02	1.03E-01	9.11E-01	7.73E-02	2.24E-01	2.83E+00	3.24E-01	1.42E-01
9	6.81E-02	8.41E-02	6.24E-02	1.57E-01	1.94E-02	1.15E+01	4.43E-01	8.46E-01	5.89E-01
10	1.29E-01	3.67E-01	2.21E-01	2.60E-01	6.13E-01	2.85E-01	9.96E-02	2.27E+00	1.49E+00

Table 4 (d): Error factor $e_{\gamma\sigma\_\text{Imaginary}}$ for Wing-Swept, mesh size 10×20

Imaginary	σ=1	2	3	4	5	7	8	9	10
γ=1	6.69E-03	1.92E-02	1.80E-02	1.10E-02	6.02E-02	8.67E-02	1.24E-01	2.69E-01	2.76E-01
2	8.67E-03	9.09E-03	2.83E-02	3.66E-02	4.36E-02	4.37E-02	1.00E-01	1.10E-01	2.38E-01
3	1.09E-03	2.87E-02	4.13E-02	3.49E-02	4.38E-02	1.80E-01	6.68E-02	1.37E-01	2.79E-01
4	1.18E-02	2.42E-02	3.55E-01	2.68E-02	7.25E-02	6.58E-02	7.40E-02	1.19E-01	1.92E-01
5	1.04E+00	1.20E-01	1.74E-02	4.02E-03	6.55E-02	1.49E-01	6.40E-04	7.10E-01	1.01E-01
7	5.36E-02	1.07E-02	9.68E-03	8.24E-02	2.27E-01	5.71E-02	1.84E-01	1.28E-01	1.14E-01
8	7.53E-02	4.30E-01	2.96E-01	9.19E-03	4.86E-02	6.05E-02	1.11E-01	6.73E-01	1.05E-01
9	2.06E-01	3.39E-02	5.80E-02	1.89E+00	8.94E-02	4.55E-01	6.38E-02	2.05E-02	4.74E-01
10	2.46E-01	5.41E-01	3.24E-01	8.35E-03	1.85E-01	3.30E-02	2.81E-02	1.92E-01	9.17E-02

Table 4 (e): Error factor $e_{\gamma\sigma\_\text{Imaginary}}$ for Wing-Swept, mesh size 20×40

Imaginary	σ=1	2	3	4	5	7	8	9	10
γ=1	2.19E-03	4.56E-03	5.85E-03	2.25E-03	3.03E-02	2.43E-01	7.90E-03	1.06E-01	1.88E-01
2	7.13E-03	1.96E-03	3.08E-02	1.33E-02	1.70E-02	1.82E-02	3.91E-02	7.67E-02	1.83E-01
3	1.65E-02	8.65E-03	1.55E-02	2.98E-02	8.20E-02	9.09E-02	3.57E-01	1.21E-02	2.96E-01
4	1.46E-02	1.03E-02	3.82E-01	1.21E-02	4.07E-02	3.29E-02	7.68E-02	8.78E-02	9.87E-02
5	1.19E+00	1.93E-02	1.59E-02	1.25E-02	4.08E-02	2.01E-01	9.65E-02	1.95E+01	3.72E-02
7	7.60E-02	2.61E-02	1.78E-02	3.99E-02	1.27E-01	4.91E-02	1.06E-01	8.73E-02	9.64E-01
8	8.75E-02	3.31E-01	2.28E-01	4.09E-02	4.36E-02	4.85E-02	1.27E-01	1.68E+00	1.09E-02
9	1.11E-01	3.10E-02	4.64E-02	9.86E-02	1.17E-01	2.17E-01	1.13E-01	1.56E-01	3.89E-01
10	2.29E-01	2.98E-01	1.56E-01	1.38E-02	5.96E-01	6.90E-02	6.23E-04	2.37E-01	1.56E-01

Table 4 (f): Error factor $e_{\gamma\sigma\_\text{Imaginary}}$ for Wing-Swept, mesh size 40×80

Imaginary	σ=1	2	3	4	5	7	8	9	10
γ=1	1.05E-03	9.23E-04	2.89E-03	5.21E-05	2.02E-02	3.74E-01	3.31E-03	7.71E-02	1.09E-01
2	6.76E-03	4.46E-03	3.26E-02	7.65E-03	9.41E-03	1.11E-02	3.67E-02	7.09E-02	1.20E-01
3	2.31E-02	4.51E-03	8.11E-03	3.31E-02	9.76E-02	5.60E-02	1.37E-01	9.91E-03	2.62E-01
4	1.37E-02	7.50E-03	6.84E-01	7.20E-03	3.29E-02	2.34E-02	6.32E-02	7.21E-02	6.32E-02
5	7.14E-01	1.75E-02	2.47E-02	1.44E-02	3.19E-02	2.19E-01	8.22E-02	1.87E+00	3.27E-02
7	9.91E-02	2.27E-02	2.24E-02	3.64E-02	1.33E-01	3.90E-02	8.97E-02	6.81E-02	3.83E-01
8	8.85E-02	2.67E-01	2.02E-01	3.76E-02	3.82E-02	3.79E-02	1.08E-01	1.19E+01	1.62E-02
9	9.61E-02	6.19E-03	1.00E-01	2.04E-01	1.09E-01	2.07E-01	1.25E-01	1.51E-01	3.60E-01
10	2.18E-01	2.04E+00	1.54E-01	2.99E-02	3.80E-01	8.36E-02	3.37E-02	1.49E+00	1.61E-01

5 CONCLUSIONS

An efficient method to calculate generalized aerodynamic forces is studied. In the proposed method, two kinds of structures are considered: one is the original structure (Str-A), and another structure (Str-B) is the one partly having different structural characteristics from the Str-A. The concept of this method is to construct the generalized aerodynamic forces for the Str-B with the Str-A's modal information and generalized aerodynamic forces. This proposed method was

applied to two models: a rectangular plate wing and the AGARD 445.6 wing. From the results, the conclusions are given as follows:

- For both models, the expression of Str-B mode vectors broadly improves as the FEM mesh size.
- The accuracy of Str-B's generalized aerodynamic forces shows better results for the Wing-Swept than those for the Wing-Rect, though the accuracy level is not enough.
- This unsatisfactoriness might be arisen from insufficient accuracy of expressing the Str-B mode vectors with those of Str-A.

For the next study, further treatment for reconstructing the Str-B mode vectors by considering artificial modal vectors should be introduced.

6 REFERENCES

[1] W. A. Silva, V. N. Vasta and R. T. Biedrom, "Development of Unsteady Aerodynamic and Aeroellastic Reduced-Order Models Using the FUN3D Code," IFASD, 2009.

[2] T. Kim, "Surrogate model reduction for linear dynamic systems based on a frequency domain modal analysis," *Computational Mechanics,* vol. 56, pp. 709-723, 2015.

[3] E. Albano and W. P. Rodden, "A Doublet Lattice Method for Calculating Lif Distributions on Oscillating Surfaces in Subsonic Flows," AIAA-68-73, 1968.

[4] M. Blair, "A Compilation of the Mathematics Leading to the Doublet Lattice Method," Wright-Patterson Air Force Base, WL-TR-92-3028, 1992.

[5] E. C. Yates, Jr., N. S. Land and J. T. Foughner, Jr., "Measured and Calculated Subsonic and Transonic Flutter Characteristics of a 45° Sweptback Wing Planform in Air and in Freon-12 in the Langley Transonic Dynamics Tunnel," NASA Langley Research Center, NASA TN D-1616, 1963.

COPYRIGHT STATEMENT